Plant Biotechnology Journal
Open Access

Plant Biotechnology Journal (2024) **22**, pp. 3229–3243 doi: 10.1111/pbi.14444

SUBSTANDARD STARCH GRAIN7 regulates starch grain size and endosperm development in rice

Haigang Yan[1,†], Yulong Ren[2,†], Binglei Zhang[3,†], Jie Jin[1], Feilong Du[1], Zhuangzhuang Shan[1], Yushuang Fu[1], Yun Zhu[2], Xin Wang[2], Changyuan Zhu[1], Yue Cai[1], Jie Zhang[1], Fan Wang[2], Xiao Zhang[1], Rongqi Wang[1], Yongxiang Wang[1], Hancong Xu[1], Ling Jiang[1], Xi Liu[1], Shanshan Zhu[2], Qibing Lin[2], Cailin Lei[2], Zhijun Cheng[2], Yihua Wang[1,4,*], Wenwei Zhang[1,4,*] and Jianmin Wan[1,2,4,*]

[1]*State Key Laboratory of Crop Genetics & Germplasm Enhancement and Utilization, Nanjing Agricultural University, Nanjing, China*
[2]*State Key Laboratory of Crop Gene Resources and Breeding, Institute of Crop Sciences, Chinese Academy of Agricultural Sciences, Beijing, China*
[3]*College of Life Sciences, Nanjing Agricultural University, Nanjing, China*
[4]*Zhongshan Biological Breeding Laboratory, Nanjing, China*

Received 12 March 2024;
revised 17 July 2024;
accepted 21 July 2024.
**Correspondence* (Tel +861082105523; fax +861082105523; email wanjianmin@caas.cn (J.W.); Tel +862584396516; fax +862584396516; email zhangww@njau.edu.cn (W.Z.); Tel +862584396628; fax +862584396628; email yihuawang@njau.edu.cn (Y.W.))
[†]These authors contributed equally to this work.

Keywords: rice (*Oryza sativa*), endosperm, starch, starch grain size, translocon.

Summary

Starch is synthesized as insoluble, semicrystalline particles within plant chloroplast and amyloplast, which are referred to as starch grains (SGs). The size and morphology of SGs in the cereal endosperm are diverse and species–specific, representing a key determinant of the suitability of starch for industrial applications. However, the molecular mechanisms modulating SG size in cereal endosperm remain elusive. Here, we functionally characterized the rice (*Oryza sativa*) mutant *substandard starch grain7* (*ssg7*), which exhibits enlarged SGs and defective endosperm development. *SSG7* encodes a plant–specific DUF1001 domain-containing protein homologous to Arabidopsis (*Arabidopsis thaliana*) CRUMPLED LEAF (AtCRL). SSG7 localizes to the amyloplast membrane in developing endosperm. Several lines of evidence suggest that SSG7 functions together with SSG4 and SSG6, known as two regulators essential for SG development, to control SG size, by interacting with translocon-associated components, which unveils a molecular link between SG development and protein import. Genetically, *SSG7* acts synergistically with *SSG4* and appears to be functional redundancy with *SSG6* in modulating SG size and endosperm development. Collectively, our findings uncover a multimeric functional protein complex involved in SG development in rice. *SSG7* represents a promising target gene for the biotechnological modification of SG size, particularly for breeding programs aimed at improving starch quality.

Introduction

Starch provides the primary source of energy in the daily diet for both humans and animals and has extensive industrial applications (Huang *et al.*, 2021). The endosperm of cereals accumulates substantial starch reserves in amyloplasts, where starch forms insoluble grains (starch grains [SGs]) that occupy most of the interior of amyloplasts. Despite the evolutionary conservation of the internal structure of SGs, native SGs display diverse sizes and morphologies depending on the plant species and organ (James *et al.*, 2003; Jane *et al.*, 1994; Matsushima *et al.*, 2010; Seung and Smith, 2019; Zhao *et al.*, 2018). Each amyloplast in rice (*Oryza sativa*) endosperm contains a single compound SG (10–20 μm in diameter) consisting of several dozen smaller non-fusing starch granules (3–8 μm in diameter). By contrast, maize (*Zea mays*) and sorghum (*Sorghum bicolor*) possess simple and uniform sizes of SGs composed of a single granule (approximately 10 μm in diameter). Barley (*Hordeum vulgare*) and wheat (*Triticum aestivum*) contain both small (less than 10 μm) and large simple SGs (approximately 15–25 μm) that coexist in the same cell (Matsushima *et al.*, 2010, 2014, 2016). As SG size is a key determinant of the suitability of starch for industrial applications, manipulating SG size is an important molecular target for bioengineering (Jobling, 2004; Lindeboom *et al.*, 2004). However, the molecular mechanism that modulates SG size in the endosperm of cereals remains unclear.

Recent studies have identified several factors modulating SG size. A reduced number of enlarged starch granules was observed in chloroplasts of Arabidopsis (*Arabidopsis thaliana*) mutants defective in STARCH SYNTHASE4 (SS4) or its interactors, including non-enzymatic proteins, which are involved in starch granule initiation in chloroplasts (Crumpton-Taylor *et al.*, 2012; Roldan *et al.*, 2007; Seung *et al.*, 2017, 2018; Vandromme *et al.*, 2019). The soft starch (*h*) locus increases SG size in maize endosperm, which is beneficial for starch processing and improving starch properties (Gutiérrez *et al.*, 2002; Wilson *et al.*, 2000). In addition, the rice *substandard starch grain4* (*ssg4*), *ssg6*, and *enlarged starch grain1* (*esg1*) mutants develop enlarged compound SGs in the endosperm (Matsushima *et al.*, 2014, 2016; Wang *et al.*, 2021). *SSG4* encodes a plastid-localized protein containing a DUF490 domain (Matsushima *et al.*, 2014). *SSG6* encodes a plastidic membrane protein homologous to aminotransferase (Matsushima *et al.*, 2016). *ESG1* encodes a putative permease subunit of a bacterial-type ATP-binding cassette (ABC) lipid transporter (Wang *et al.*, 2021). These three proteins also affect the size of chloroplasts but not the SGs within them. However, their precise modes of action and molecular mechanisms in determining SG size remain obscure.

Notably, Arabidopsis TIC236, the homologue of rice SSG4, functions in chloroplast development by linking the TOC (translocon on the outer chloroplast membrane) and TIC (translocon on the inner chloroplast membrane) complexes, which orchestrate protein import in chloroplasts (Chen *et al*., 2018; Jarvis and López-Juez, 2013; Richardson and Schnell, 2020).

Arabidopsis *CRUMPLED LEAF* (*AtCRL*) encodes a plastidic outer envelope membrane protein containing a DUF1001 domain that functions in cell division, cell differentiation, and plastid division (Asano *et al*., 2004). *crl* cells contain a reduced number of enlarged plastids, and *crl* plants display morphological abnormalities. AtCRL is homologous to the cyanobacterial phycocyanobilin T-type (CpcT) lyases, which function in phycobilisome biogenesis by covalently attaching phycocyanobilin (PCB) to antenna proteins (Shen *et al*., 2006). AtCRL homologues are present in various plant species but not in yeast (*Saccharomyces cerevisiae*) or animals. Whether AtCRL homologues function in SG formation and endosperm development in cereals remains unclear.

In this study, we isolated and characterized the rice floury endosperm mutant *ssg7*, which develops enlarged SGs in starch-accumulating tissues. *SSG7* encodes a DUF1001 domain-containing protein homologous to AtCRL. Our combined biochemical and genetic evidence suggest that SSG7 interacts with SSG4 and SSG6, and they function in SG development by associating with TOC or TIC components in rice. *SSG7* represents a promising target gene for modifying SG size, particularly for breeding programs aimed at improving starch quality.

Results

Aberrant SG development in *ssg7* endosperm

To dissect the molecular machinery involved in SG development in rice, we identified *ssg7*, a mutant with defective endosperm development, from an *N*-methyl-*N*-nitrosourea-mutagenized pool of *japonica* rice cultivar W017. Whereas wild-type endosperm is translucent, the *ssg7* mutant develops floury-white endosperm (Figure 1a,b), which was apparent in developing grains beginning approximately 18 days after flowering (DAF) and in mature polished grains (Figure S1a,b). Scanning electron microscopy (SEM) showed that mature *ssg7* endosperm contained spherical and loosely packed SGs, in sharp contrast to the polyhedral and tightly-packed SGs in wild-type endosperm (Figure 1c). Iodine-stained semi-thin sections of mature *ssg7* endosperm clearly showed enlarged SGs, the area of which was approximately 4-fold larger than that in the wild type (Figure 1d,e). However, the starch content was significantly lower in *ssg7* grains than in the wild type (Figure 1f). We next examined the starch composition and the fine structure of amylopectin in *ssg7* grains. Consistent with the declined starch accumulation, the amylose content was also significantly reduced (Figure S1c), indicating the altered starch composition in *ssg7* grains. Analysis of the chain length distribution (CLD) of *ssg7* amylopectin revealed an increase in the number of chains with a degree of polymerization (DP) of 6–8 branches and a decrease in the number of chains with a DP of 9–20 (except for DP13) branches (Figure S1d). The viscosity pattern of starch in *ssg7* endosperm was largely similar to that of wild-type starch but with reduced viscosity (Figure S1e), indicating that the physicochemical characteristics of the *ssg7* starch were altered.

The *ssg7* mature grains also exhibited reduced protein and lipid accumulation, indicating an important role of the *SSG7* locus in storage substance accumulation (Figure S1f,g). Accordingly, the mature grain weight of *ssg7* decreased by 12.78% compared to that of the wild type, which is consistent with a lower grain-filling rate (Figure 1g; Table S1). In addition, *ssg7* plants exhibited no visible differences from wild-type plants at the vegetative stage, such as plant height and tiller number, but they exhibited a markedly reduced seed setting rate (Table S1). Collectively, the *ssg7* mutation causes pleiotropic effects on reproductive development.

SSG7 plays a crucial role in modulating SG size

To investigate SG development in *ssg7* endosperm, we performed cytohistological analyses of developing grains by examining periodic acid-Schiff (PAS) and Coomassie Bright Blue (CBB) double-stained semi-thin sections. Enlarged SGs (stained red by PAS) and protein bodies (stained blue by CBB) were apparent in *ssg7* endosperm cells at 6 DAF (Figure 2a). At 9 DAF, we observed markedly reduced numbers of even larger SGs and smaller protein bodies, together with large air spaces, in the aleurone layer and starchy endosperm cells of *ssg7* (Figure 2b), which is consistent with the reduced accumulation of storage substances in the mutant (Figures 1f and S1f).

To investigate when SG enlargement occurs in *ssg7* endosperm, we analysed early-developing grains at 3, 6, and 9 DAF. Enlarged SGs were visible as early as 3 DAF in *ssg7* endosperm, occupying an area that was more than 1.7-fold larger than that of wild-type SGs. At 6 and 9 DAF, the area occupied by enlarged SGs was more than 2.8- and 3.2-fold larger in *ssg7* than the wild type, respectively (Figure 2c,d). By contrast, the size of starch granules in *ssg7* was comparable to that in the wild type during endosperm development (Figure 2e). Therefore, the enlargement of SGs was due to an increased number of starch granules per SG in *ssg7*, suggesting that more granule initiation events likely occurred in a single amyloplast. Notably, clusters of smaller SGs coexisted with the enlarged SGs in *ssg7* endosperm cells at 9 DAF (Figure 2c), as observed in the previously reported *ssg6* mutant (Matsushima *et al*., 2016). Quantitative analysis revealed that the total numbers of SGs and granules per area were lower in *ssg7* than in the wild type (Figure S2), in agreement with the reduced starch content in *ssg7* (Figure 1f). In addition, the enlarged SGs in *ssg7* were more spherically shaped (Figure 2c), as observed in *ssg4*, *ssg6*, and *esg1* mutants (Matsushima *et al*., 2014, 2016; Wang *et al*., 2021).

As endosperm is a triploid tissue, F_1 grains with different doses of the *SSG7* allele can be generated by performing reciprocal crosses between the wild type and *ssg7*. The appearance of endosperm and the sizes of SGs in the two reciprocal F_1 hybrid grains were similar to those of the wild type (Figure S3), indicating that the *SSG7* allele has no apparent gene dosage effect on regulating SG size.

We also observed enlarged SGs in pollen grains and young pericarp of *ssg7* (Figure S4). Unexpectedly, unlike the *ssg4*, *ssg6*, and *esg1* mutants (Matsushima *et al*., 2014, 2016; Wang *et al*., 2021), *ssg7* plants developed normal leaves with similar chloroplast areas compared to those of the wild type, although some chloroplasts appeared more spherical than normal (Figure S5). Altogether, these results suggest that the *ssg7* mutation affects SG development in rice.

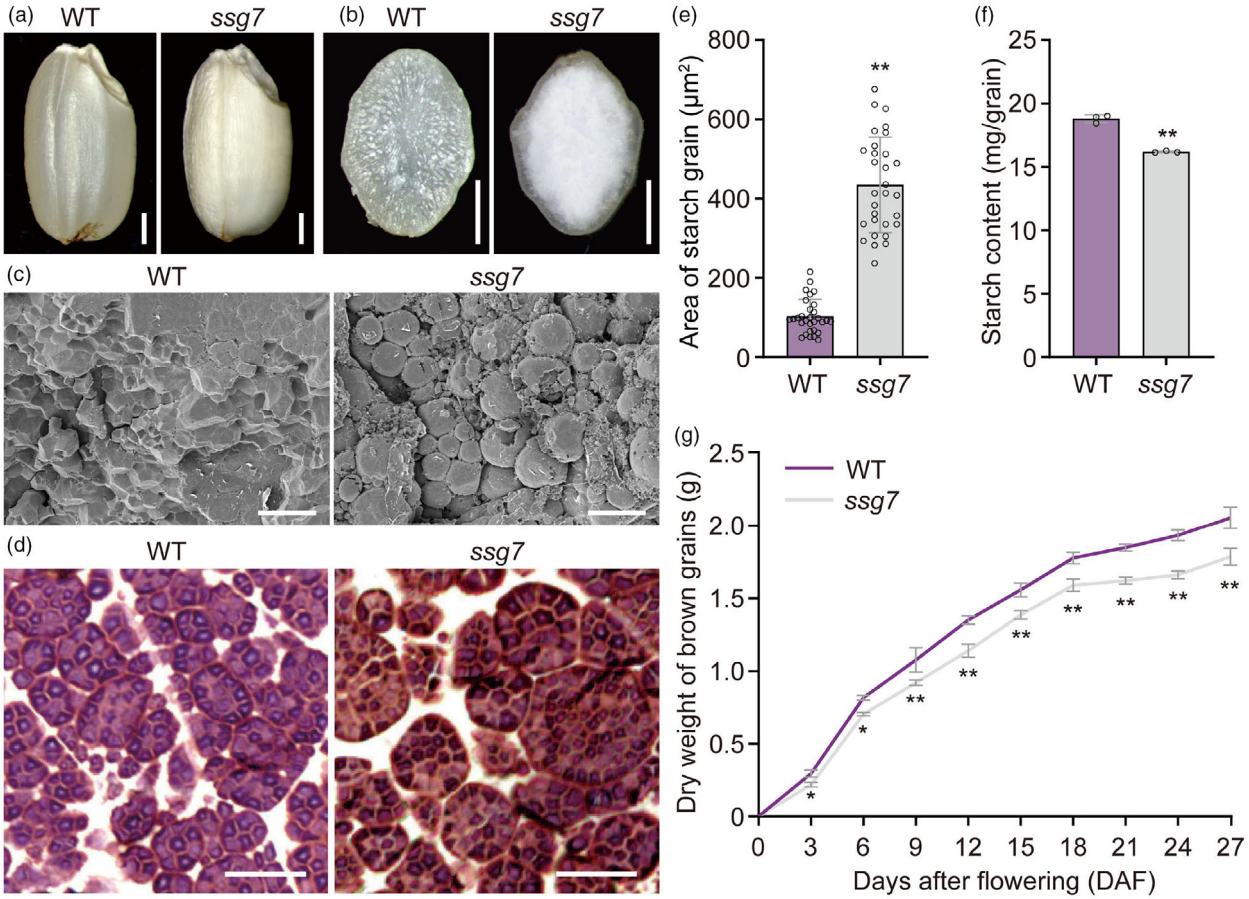

Figure 1 Aberrant SG development in *ssg7* endosperm. (a) Representative images of wild-type (WT) and *ssg7* mature grains. Bars = 1 mm. (b) Transverse sections of the representative WT and *ssg7* mature grains. Bars = 1 mm. (c) Scanning electron microscopy (SEM) images of transverse sections of the representative WT and *ssg7* mature grains. Bars = 20 μm. (d) Iodine-stained semi-thin sections prepared from WT and *ssg7* mature grains. Bars = 20 μm. (e) Quantification of the areas occupied by starch grains (SGs) in WT and *ssg7* mature endosperm (n = 30). (f) Total starch contents in mature grains of WT and *ssg7* (n = 3). (g) Dry substance accumulation profiles of WT and *ssg7* developing grains. Data showed the weight of 100 brown grains (n = 3). Values are means ± SD. *P < 0.05, **P < 0.01 by Student's t-test.

SSG7 encodes an AtCRL homologue and is generally expressed in rice

Genetic analysis indicated that the *ssg7* mutation behaves as a single recessive allele (Table S2). To clone the causal gene responsible for the *ssg7* phenotypes, we constructed an F_2 segregating population by crossing *ssg7* with the *indica* cultivar N22. Using 528 F_2 homozygous *ssg7* individuals, the *ssg7* locus was delimited to a 158-kb genomic interval flanked by the simple sequence repeat (SSR) markers RM229 and Yhg-5 on chromosome 11 (Figure 3a). Annotation of this 158-kb genomic region identified 17 putative open reading frames (ORFs; Figure 3a). Sequencing analysis revealed a single nucleotide substitution adjacent to the splicing donor site of the 7th intron of LOC_Os11g32160, leading to alternative splicing in *ssg7* (Figure 3b,c). We detected two distinct transcripts from *ssg7* grains by RT-PCR analysis. The major transcript was found to retain 132 bp of intron 7, which was predicted to result in a frameshift and a premature stop codon, while the minor transcript corresponded to the wild-type transcript (Figure 3b–d).

We conducted a complementation test by introducing the coding sequence of LOC_Os11g32160 driven by the *UBIQUITIN* promoter into *ssg7* calli. As anticipated, transgene-positive grains exhibited a wild-type translucent appearance and developed normal-sized SGs (Figures 3e,f and S6). Furthermore, we performed CRISPR/Cas9 gene editing to knock out LOC_Os11g32160. The knockout mutant *KO1*, with a 21-bp deletion in LOC_Os11g32160, phenocopied *ssg7*, while two other mutants with frameshift mutations, named *KO2* and *KO3*, were heterozygous at this locus, most likely due to defects in male gamete transmission (Figure S7a,b). Notably, pollen from the heterozygous *KO2* plant was segregated with respect to SG morphology (Figure S7c). The segregation ratio of pollen containing simple or compound SGs was approximately 1:1 (Figure S7d), indicating a specific role of *SSG7* in the compound SG formation. We raised polyclonal antibodies against SSG7, which specifically recognized a predicted ~30-kD band in total protein extracts from developing grains of wild-type and transgenic overexpression plants, but not the knockout mutant *KO1* (Figure 3g). Little endogenous SSG7 protein was detected in *ssg7*, consistent with the low abundance of normal transcripts (Figures 3d,g and S8). Taken together, these results substantiate that LOC_Os11g32160 corresponds to the *SSG7* gene.

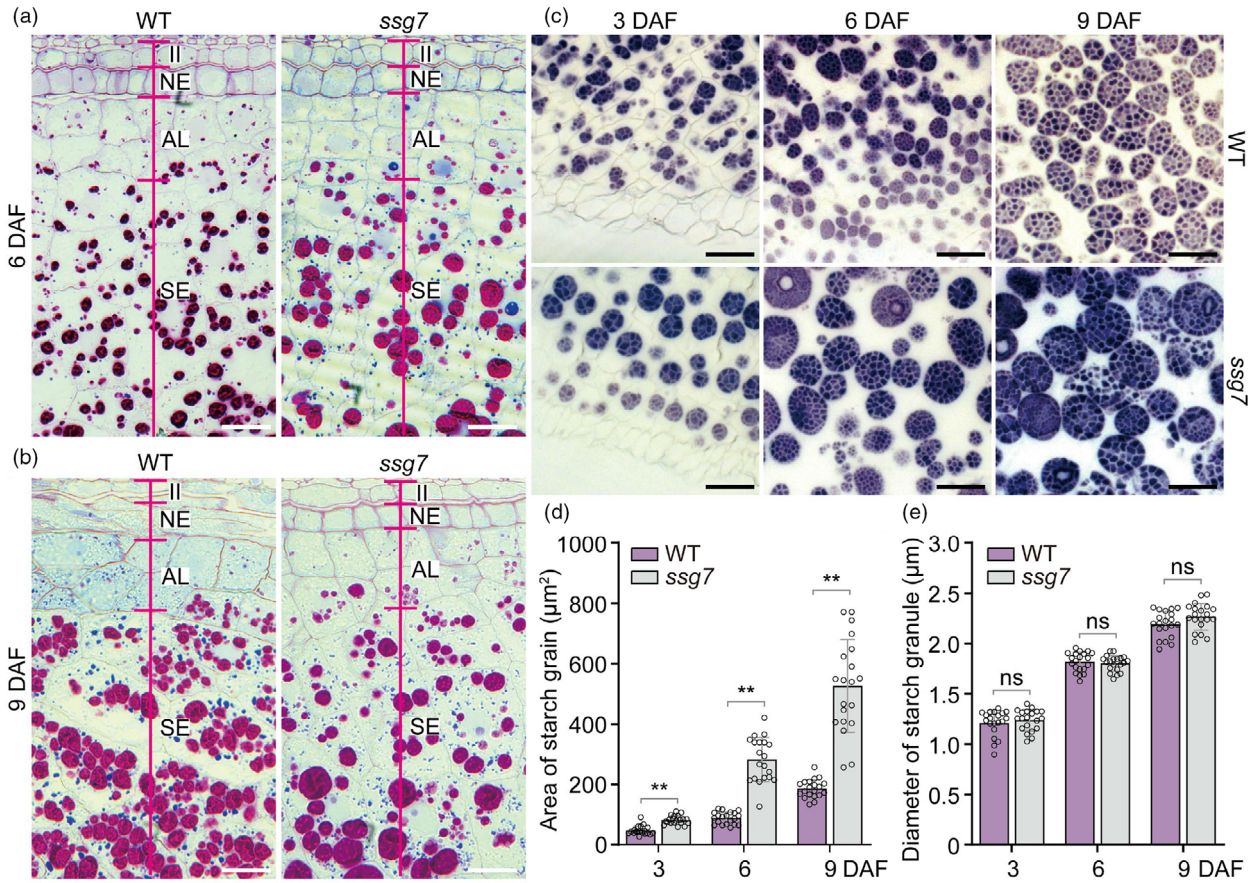

Figure 2 The *ssg7* mutation affects starch grain development. (a, b) Light microscopy images of periodic acid-Schiff (PAS) and Coomassie Bright Blue (CBB) double-stained semi-thin sections prepared from developing endosperm of the wild type (WT) and *ssg7* at 6 (a) and 9 (b) DAF. DAF, days after flowering. II, inner integument; NE, nucellar epidermis; AL, aleurone layer; SE, starchy endosperm cells. Bars = 20 μm. (c) Iodine-stained semi-thin sections prepared from developing endosperm of WT and *ssg7* at different stages. Bars = 20 μm. (d) Quantification of the areas occupied by starch grains (SGs) in semi-thin sections of WT and *ssg7* developing endosperm from 3 to 9 DAF in (c) (n = 20). Note that the quantification does not contain the very small SGs. (e) Measurement of the diameters of starch granules in WT and *ssg7* developing endosperm in (c) (n = 20). Values are means ± SD. $^{**}P < 0.01$ by Student's t-test. ns, no significance.

SSG7 is predicted to encode a protein of 275 amino acids that harbours a putative transmembrane domain and a large DUF1001 domain (Figure S9a). Phylogenetic analysis indicated that *SSG7* is a single copy gene in the rice genome that is homologous to *AtCRL* (Figure S9b; Asano *et al.*, 2004). Notably, the function of SSG7 could have diverged from that of cyanobacterial CpcT lyase, as evidenced by their low sequence identity (Figure S9b,c). Supporting this notion, overexpressing *AtCRL* or cyanobacterial *CpcT* in the *ssg7* background did not rescue the *ssg7* mutant phenotypes (Figures 3e–g and S6). These data suggest that functional divergence has extensively occurred among *AtCRL* homologues during evolution.

We then used the anti-SSG7 antibodies to analyse the accumulation pattern of SSG7 via immunoblot analysis of total protein extracts from different tissues of wild-type plants. SSG7 was widely present in all tissues examined, with the highest accumulation in leaf and stem tissues (Figure 3h). In developing endosperm, SSG7 remained abundant until the late stage of development (Figure 3h). Together, these data suggest that *SSG7* encodes the AtCRL homologue in rice and it is broadly expressed in various tissues.

SSG7 localizes to the amyloplast membrane and can form homodimers

To investigate the subcellular localization of SSG7, we separately introduced two fusion constructs into *ssg7* calli: constructs harbouring *SSG7-GFP* (*Green fluorescent protein*, fused with the C terminus of SSG7) or *GFP-SSG7* (GFP fused with the N terminus of SSG7) driven by its native promoter. The phenotypes of transgenic grains harbouring GFP-SSG7 but not SSG7-GFP fusion protein were restored to the wild-type level (Figure S10), indicating that the GFP-SSG7 fusion protein was biologically functional *in vivo*. Unfortunately, we failed to detect any fluorescent signals in developing endosperm, most likely due to low abundance of SSG7 in developing endosperm tissue (Figure 3h). As an alternative, we introduced *GFP-SSG7* driven by the *UBIQUITIN* promoter into *ssg7* calli, and the results showed that the transgene-positive grains exhibited wild-type phenotypes (Figure S11). Given the predicted transmembrane domain in SSG7 and the defective SG development in *ssg7* endosperm (Figures 1c,d, 2a–c and S9a), we reasoned that SSG7 might be an amyloplast membrane-localized protein. As expected, GFP-SSG7

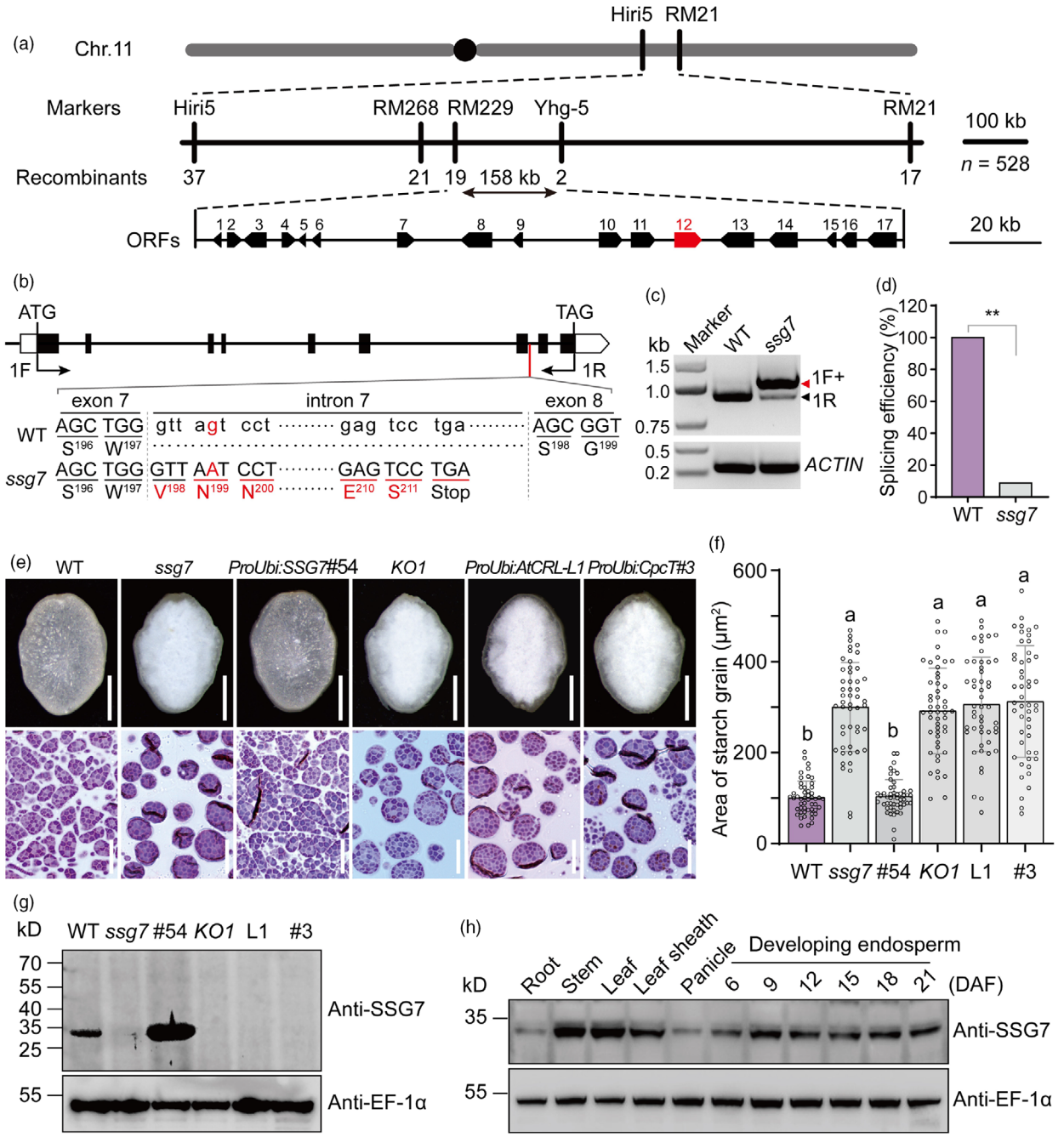

Figure 3 Map-based cloning of the *SSG7* gene and characterization of the SSG7 protein. (a) Fine mapping of the *SSG7* locus. The *SSG7* locus was narrowed to a 158-kb interval on chromosome 11. The numbers under vertical lines and blocks at the bottom indicate the recombinant plants and candidate genes, respectively. Note that the *SSG7* gene was highlighted in red. Chr, chromosome; ORFs, open reading frames. (b) Genomic structure and the mutation site of *SSG7*. Exons are shown as boxes, and introns as lines. The position of start (ATG) and stop (TAG) codons are indicated. A G-to-A substitution occurred in the 7th intron of *SSG7*, leading to alternative splicing in *ssg7*. WT, wild type. (c) Determination of *SSG7* transcripts in WT and *ssg7*. The unspliced transcript containing the 7th intron was indicated by a red arrowhead, whereas the spliced WT-like transcript was indicated by a black arrowhead. The primer pair (1F + 1R) in (b) was used for amplification. Rice *Actin* gene was used as an internal control. (d) Effect of the *ssg7* mutation on splicing efficiency. RT-PCR products from three independent experiments were subjected to sequence analysis to assess the splicing efficiency. $^{**}P < 0.01$ by Student's *t*-test. (e) Rescue of grain appearance (upper panels) and starch grain (SG) sizes (lower panels) of *ssg7* by overexpressing *SSG7* driven by the *UBIQUITIN* promoter, while a knockout mutant *KO1* carrying a 21-bp deletion phenocopied the *ssg7* mutant. Phenotypes of *AtCRL* and *CpcT* overexpression grains in the *ssg7* background were not recovered. Bars = 1 mm in upper panels, 20 μm in lower panels. (f) Quantification of the areas occupied by SGs in developing endosperm of WT, *ssg7*, and transgenic plants. Values are means ± SD ($n = 25$). $P < 0.05$ by Duncan's multiple range tests. Note that the quantification does not contain the very small SGs. (g) SSG7 antibodies could specifically detect endogenous SSG7 protein in total protein extracts from WT and *SSG7* overexpression lines, but not in *ssg7* and other transgenic plants, as indicated. EF-1α was used as a loading control. (h) Protein accumulation profiles of SSG7 in various tissues and developing endosperm. DAF, days after flowering. EF-1α was used as a loading control.

exhibited a ring-like localization pattern with its GFP signals surrounding the developing SGs in developing endosperm cells (Figure 4a), verifying that SSG7 may be an amyloplast membrane-localized protein. When coexpressed with fluorescent marker proteins either for the plastid outer envelope membrane (OEP7-DsRed) or for the inner envelope membrane (BRITTLE-1 [BT1]-DsRed) (Kawagoe, 2013; Yun and Kawagoe, 2010), confocal microscopy analyses revealed that GFP-SSG7 co-localized well with OEP7-DsRed but not with BT1-DsRed in developing subaleurone cells of rice endosperm (Figure 4b,c).

To further verify the intracellular localization of SSG7 in developing endosperm, we conducted immuno-gold electron microscopy of ultrathin sections prepared from developing endosperm of GFP-SSG7-complemented lines using the primary anti-GFP antibody in combination with 10-nm gold particle-coupled secondary antibodies. Consistent with our confocal microscopic observations (Figure 4a,b), the gold particles were largely detected on the surfaces of SGs (Figure 4d). Furthermore, the subcellular fractionation assay showed that SSG7 was enriched in the membrane-associated pellet fraction (Figure 4e), and was able to be extracted from the pellet fraction after detergent treatment but not NaCl or Na_2CO_3 treatment (Figure 4f). Taken together, these results indicate that SSG7 is an integral membrane protein of amyloplasts.

AtCRL has been shown to be able to form homodimers *in vivo* and *in vitro* (Wang *et al*., 2020). To test whether rice SSG7 could form homodimers, we performed a yeast two-hybrid assay and confirmed that SSG7 could interact with itself. Consistent with this result, a firefly luciferase complementation imaging (LCI) assay in leaf epidermal cells of *Nicotiana benthamiana* and an *in vivo* coimmunoprecipitation (Co-IP) assay in rice protoplasts confirmed that SSG7 is able to form homodimers (Figure 4g–i).

SSG7 associates with SSG4 and SSG6

To dissect the molecular mechanism by which *SSG7* modulates SG development, we performed immunoprecipitation coupled to mass spectrometry (IP-MS) using protein extracts from developing endosperm of transgenic plants expressing either GFP-SSG7 or free GFP. We subjected the immunoprecipitates to SDS-PAGE, followed by CBB staining (Figure 5a) and LC–MS/MS analysis (Data S1). Intriguingly, we detected SSG4 and SSG6, known as two important regulators essential for SG development (Matsushima *et al*., 2014, 2016), in the GFP-SSG7 precipitate but not in the free GFP precipitate (Figure 5b), suggesting that SSG7 forms a functional protein complex with SSG4 and SSG6 to regulate SG development. We verified the interaction between SSG7 and SSG6 by immunoblot analysis of the GFP-SSG7 precipitate and an *in vivo* LCI assay in leaf epidermal cells of *N. benthamiana* (Figure 5c,d).

Due to the strong inhibition of the full-length *SSG4* sequence on bacterial growth (Matsushima *et al*., 2014), we failed to clone the full-length *SSG4* gene. A previous study from Arabidopsis SSG4 homologue TIC236 showed that it is an integral inner envelope membrane protein, and could directly interact with the outer envelope membrane protein TOC75 via its C-terminal DUF490 domain localized in the intermembrane space (Figure S12a; Chen *et al*., 2018). Interestingly, protein topology prediction showed that the C-terminal DUF1001 domain of SSG7 might be exposed to the intermembrane space (Krogh *et al*., 2001). Based on these clues, we proposed that SSG7 might interact with SSG4 in a manner similar to that of Arabidopsis TOC75 (Chen *et al*., 2018). To verify this notion, we performed an *in vitro* pull-down assay, and found that His-DUF490 could bind to glutathione S-transferase (GST)-DUF1001 but not to free GST (Figure 5e). This interaction was largely compromised when the last 16 amino acid residues of the DUF490 domain were truncated (Figure 5e,f), which is in agreement with the effects of the C-terminal tail of the DUF490 domain on protein–protein interactions (Chen *et al*., 2018; Selkrig *et al*., 2012). Collectively, these results indicate that SSG7 forms a functional protein complex with SSG4 and SSG6 to regulate SG development in rice.

SSG7 physically interacts with the translocon complex

It is reported that Arabidopsis TIC236/SSG4 functions in plastid development by linking the TOC and TIC complexes (Chen *et al*., 2018). We proposed that SSG4 and SSG7 might also be associated with translocons in rice. Consistent with this proposition, our LC–MS/MS assay indeed detected diverse TOC core components in the GFP-SSG7 precipitate (Figure 6a). They included TOC159, TOC120, TOC90, TOC75, TOC64, and TOC34, with the highest protein score obtained for TOC75. Furthermore, immunoblot analyses of the GFP-SSG7 precipitate using protein-specific antibodies confirmed the presence of TOC34 and TOC75 (Figure 6b). A small number of peptides for TIC110, known as a core component of the TIC complex (Jackson

Figure 4 SSG7 localizes to the amyloplast membrane and can form homodimers *in planta*. (a) Representative confocal microscopy images showing that GFP-SSG7 localizes to the periphery of amyloplasts and exhibits numerous ring-like structures in developing subaleurone cells. Bars = 10 μm. (b, c) Representative confocal microscopy images showing that GFP-SSG7 largely co-localizes with OEP7-DsRed (b), but not BT1-DsRed (c) in developing subaleurone cells. Bars = 10 μm. (d) Immuno-gold localization of GFP-SSG7 in transgenic subaleurone cells. Ultrathin sections were prepared from HPF/FS samples of transgenic complemented GFP-SSG7 grains, followed by hybridization with the monoclonal GFP antibody in combination with 10-nm gold particle-coupled secondary antibodies. The black boxes are the selected regions for magnification. Red arrows indicate the gold particles. SG, starch grain. Bars = 2 μm in panel 1; 200 nm in panel 2. (e) Subcellular fractionation assays showed that SSG7 is a membrane protein. Total protein was extracted from wild-type developing endosperm, followed by centrifugation and fractionation into supernatant (S100, soluble fraction) and pellet (P100, membrane-associated fraction). Both fractions were subjected to immunoblot analyses with antibodies against SSG7, an amyloplast outer envelope membrane protein TOC75, and a cytosol protein UDP-glucose pyrophosphorylase (UGPase), respectively. (f) SSG7 is an integral membrane protein. The P100 fraction was resuspended with the different buffers and fractionated into supernatant (S) and pellet (P) fractions. Immunoblot analyses were performed with anti-SSG7 and anti-TOC75 antibodies, respectively. (g) Yeast two-hybrid assay showing that SSG7 variant with a deletion of the TM domain interacts with itself. DDO, SD/-Trp/-Leu; QDO, SD/-Trp/-Leu/-His/-Ade. TM, putative transmembrane domain. (h) Firefly luciferase complementation imaging (LCI) assay showing that SSG7 forms a homodimer in leaf epidermal cells of *N. benthamiana*. NL, N terminus of LUC; CL, C terminus of LUC. (i) Co-immunoprecipitation (Co-IP) assay confirmed the association of SSG7 with itself. Rice protoplasts expressing GFP-SSG7 or free GFP with Flag-SSG7 were subjected to total extraction and IP with GFP magnetic beads followed by immunoblot analysis with anti-GFP and anti-Flag antibodies, respectively.

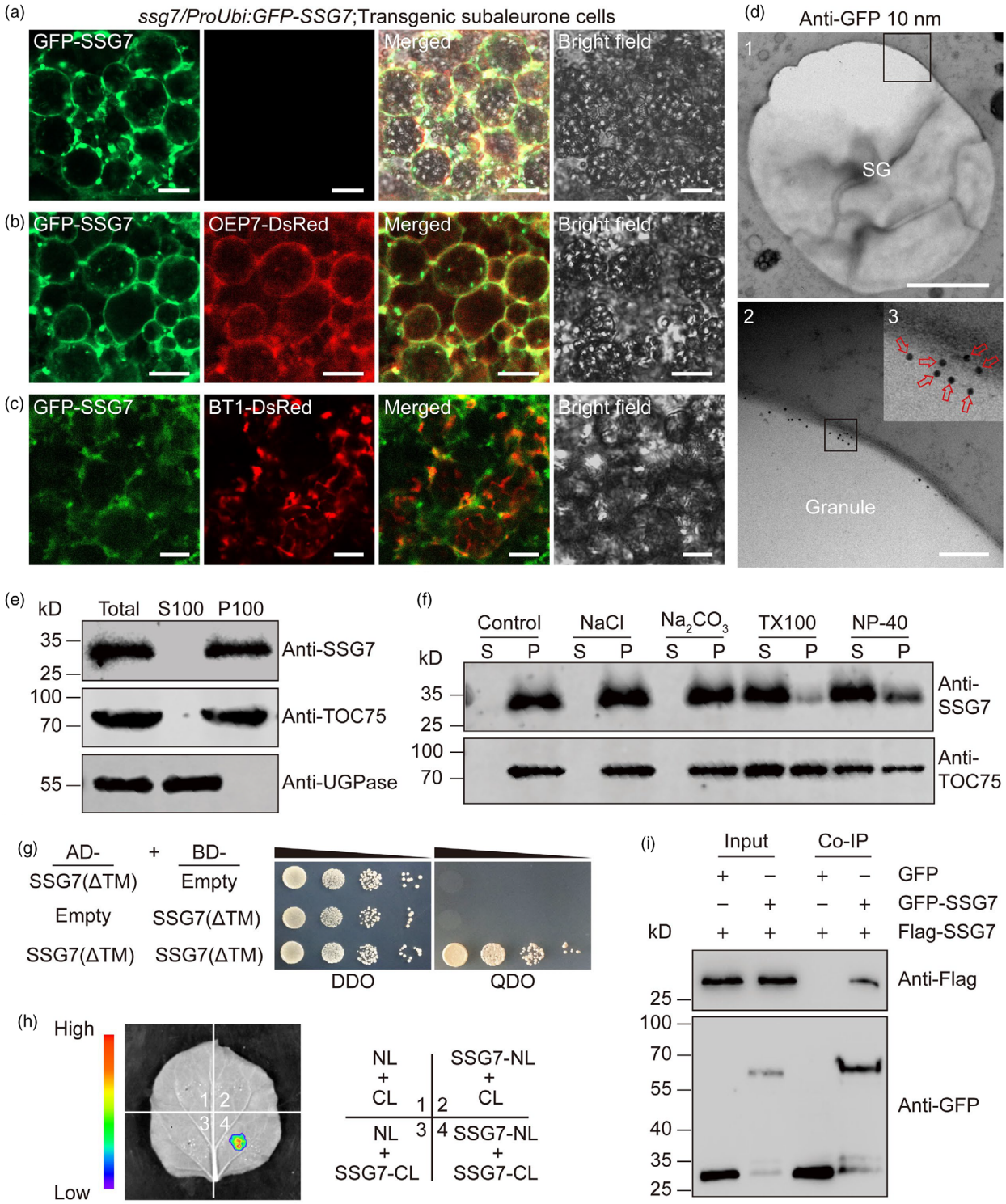

et al., 1998), were also specifically detected in the GFP-SSG7 precipitate (Figure 6a). In addition, immunoblot analyses showed that the protein abundances of TOC75 and TOC34 were decreased by 37.5% and 56.5% in developing *ssg7* grains, respectively, compared to the wild type (Figure 6c,d). These results, combined with the finding that SSG7 interacts with SSG4 and SSG6, suggest that SSG7 functions together with SSG4 and SSG6 in regulating SG development via their association with translocons.

SSG7 genetically interacts with *SSG4* and *SSG6* to modulate SG development

We tried to investigate genetic relationship of *SSG7* with *SSG4* and *SSG6*. A recent study showed that a gain-of-function mutation of *TIC236/SSG4* could rescue the chloroplast developmental defect of the Arabidopsis *crl/ssg7* mutant (Fang *et al.*, 2022). However, due to the unavailable full-length *SSG4* gene (Matsushima *et al.*, 2014), we could not overexpress

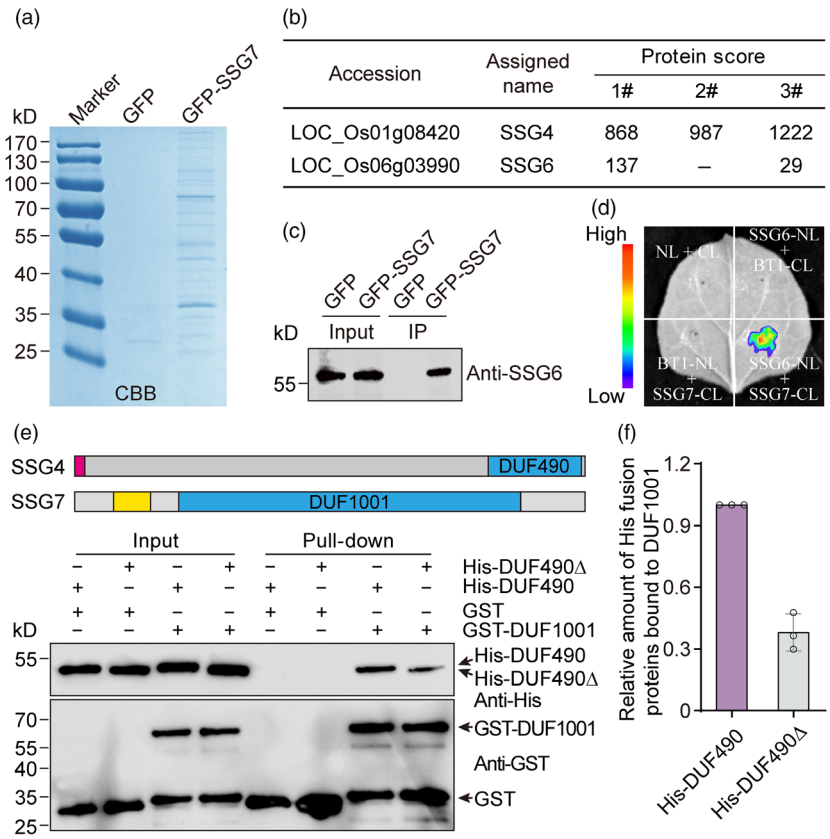

Figure 5 SSG7 interacts with both SSG4 and SSG6. (a) CBB-stained SDS-PAGE gel. Developing endosperm of transgenic rice expressing either GFP-SSG7 or free GFP driven by the *UBIQUITIN* promoter was used for protein extraction. The extracts were separately incubated with GFP μMACS Microbeads and the bound proteins were subjected to SDS-PAGE analysis. CBB, Coomassie Brilliant Blue. (b) Summary of proteins co-precipitated with GFP-SSG7 and identified by mass spectrometry. (c) Immunoblot analysis of the GFP-SSG7 immunoprecipitate samples obtained from developing endosperm of transgenic rice with antibodies against SSG6. (d) Firefly luciferase complementation imaging (LCI) assay showing that SSG7 specifically associates with SSG6 in leaf epidermal cells of *N. benthamiana*. NL, N terminus of LUC; CL, C terminus of LUC. BT1 was used as a negative control. (e) *In vitro* GST pull-down assay showing that GST-tagged DUF1001 domain of SSG7 but not free GST can pull down His-tagged C-terminal DUF490 domain of SSG4. The structures of SSG4 and SSG7 proteins were shown. The DUF1001 domain of SSG7 and the C-terminal DUF490 domain of SSG4 are highlighted in blue. The red box and yellow box represent the signal peptide of SSG4 and putative transmembrane domain of SSG7, respectively. The grey boxes represent the regions of SSG4 and SSG7 proteins containing no previously annotated domains. Note that a deletion of the C-terminal tail of the DUF490 domain largely compromised this interaction. Black arrows indicate the corresponding recombinant proteins. DUF, domain of unknown function. (f) Quantification of the relative amounts of His fusion proteins bound to GST-DUF1001. The intensity of pulled-down His-DUF490Δ was normalized by the intensity of pulled-down His-DUF490 using Image J software from three independent experiments.

SSG4 in the *ssg7* background. Alternatively, we crossed *ssg4* with *ssg7* in an attempt to generate a *ssg4 ssg7* double mutant (Figure S12; Table S3). Unfortunately, we failed to obtain a homozygous *ssg4 ssg7* double mutant, most likely due to the impaired transmission efficiency of male gametophytes (Figure 7a,b). Consistent with the phenotype observed in the *KO2* line of *SSG7*, the segregation ratio of pollen grains containing simple SGs (resembling single mutants) versus enlarged compound SGs (likely $ssg4^{-/-}$ $ssg7^{-/-}$) was close to 1:1 in $ssg4^{+/-}$ $ssg7^{-/-}$ and $ssg4^{-/-}$ $ssg7^{+/-}$ plants (Figure 7c,d). These data suggest that *SSG4* and *SSG7* function synergistically to modulate SG development in rice.

We next investigated the genetic interaction between *SSG7* and *SSG6*. Notably, when *SSG6* was overexpressed in the *ssg7* mutant, the transgenic grains exhibited translucent endosperm and normal-sized SGs (Figures 7e,f and S13), suggesting that SSG6 and SSG7 share partial functional redundancy in regulating SG size in rice endosperm.

Discussion

SSG7 is particularly required for compound SG formation in rice

Starch grains size is a vital property for the industrial applications of starch, including the production of both food and non-food products. Increased SG size could improve starch yield from maize and cassava (*Manihot esculenta*) during processing (Gutiérrez *et al.*, 2002). Small SGs could be utilized as a fat substitute and for manufacturing degradable plastic film, emphasizing the importance of SG size for industrial applications (Lindeboom *et al.*, 2004; Malinski *et al.*, 2003). An in-depth understanding of the molecular mechanism that governs SG size in crops is thus important.

Numerous rice mutants with altered endosperm starch synthesis have been identified and characterized. Most mutants defective in carbohydrate metabolism generally develop reduced

(a)

Accession	Assigned name	Protein score		
		1#	2#	3#
LOC_Os05g05950	TOC159	2821	2195	2436
LOC_Os10g40110	TOC120	817	457	593
LOC_Os12g09570	TOC90	187	86	98
LOC_Os03g16440	TOC75	4314	3762	3667
LOC_Os03g50010	TOC64	61	52	31
LOC_Os03g13730	TOC34	716	1108	518
LOC_Os10g35010	TIC110	-	27	29

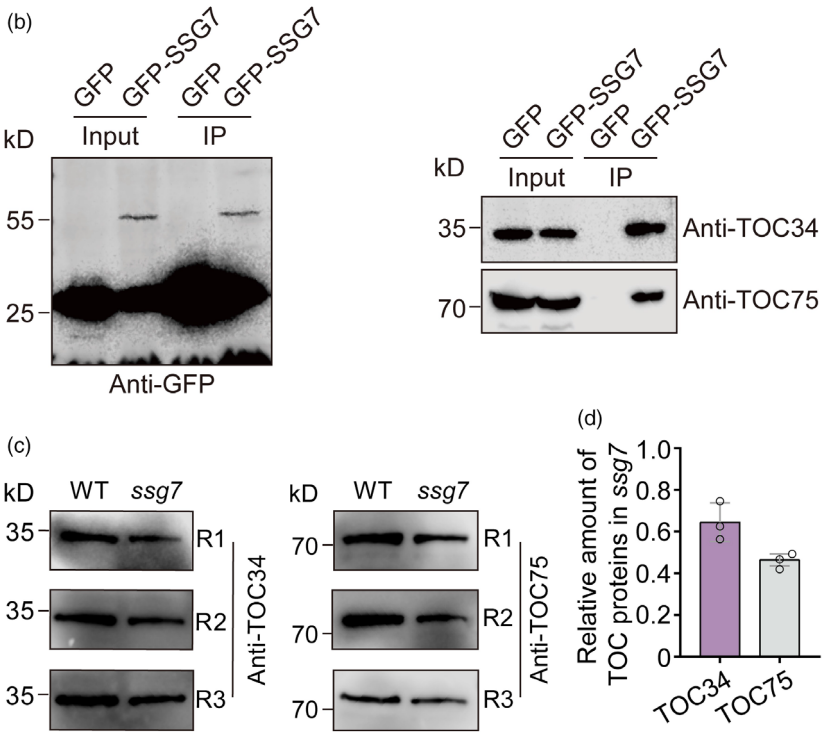

Figure 6 SSG7 interacts with the translocon components. (a) Summary of proteins co-precipitated with GFP-SSG7 and identified by mass spectrometry. Developing endosperm of transgenic rice expressing either GFP-SSG7 or free GFP driven by the *UBIQUITIN* promoter was used for protein extraction. (b) Immunoblotting of the GFP-SSG7 immunoprecipitate samples obtained from developing endosperm of transgenic rice with antibodies against translocon components. (c) Immunoblot analysis of total extracts from developing grains of the wild type (WT) and *ssg7* using antibodies against TOC34 and TOC75, respectively. Equivalent volumes of total protein extracts from the same weight of grains were loaded in each lane. R1 to R3 indicate three times independent experiments. (d) Quantification of the relative amounts of translocon components in the *ssg7* mutant. The intensity of translocon components in *ssg7* was normalized by the corresponding intensity of those in WT using Image J software.

size of SGs (Matsushima *et al.*, 2010). By contrast, the rice *ssg4*, *ssg6*, and *esg1* mutants develop enlarged chloroplasts and amyloplasts (SGs), resulting in abnormal leaf colour and chalky endosperm (Matsushima *et al.*, 2014, 2016; Wang *et al.*, 2021). In this study, we identified a rice *ssg7* mutant containing enlarged spherical SGs in various starch-accumulating tissues (Figures 1c,d, 2a–c and S4). Distinct from the Arabidopsis *crl* mutant that exhibits pleiotropic phenotypes at the vegetative stage (Asano *et al.*, 2004), the loss of *SSG7* particularly influences SG development in starch-accumulating tissues.

During *ssg7* endosperm development, a growing number of tiny SGs coexisted with enlarged SGs in the same cell, as observed in *ssg6* and *esg1* (Matsushima *et al.*, 2016; Wang *et al.*, 2021). Nevertheless, *esg1* endosperm also contains small, weakly stained compound SGs, which were not observed in *ssg4*, *ssg6*, or *ssg7* endosperm, suggesting that *ESG1* functions in compound SG formation in a manner distinct from that of the other three *SSG* genes (Wang *et al.*, 2021). The functional interaction among three SSG proteins observed in our study supports this notion (Figures 5 and 6). Furthermore, *SSG4* has been proposed to control SG size in diverse starch-accumulating tissues, like *SSG7*, although the requirement for SSG6 activity in modulating SG size varies in different tissues (Matsushima *et al.*, 2016). Compared to the slightly chalky *ssg6* grains, both *ssg4* and *ssg7* grains were highly chalky, which is consistent with the severely impaired starch biosynthesis (Figure 1f; Matsushima *et al.*, 2014). Notably,

(a)
Genetic analysis of gametic transmission efficiency of heterozygous *ssg4*$^{+/-}$ *ssg7*$^{-/-}$ plants

Combinations (♀ × ♂)	F_1 genotypes		χ^2value (*P*) for 1:1 segregation	TE
	ssg4$^{+/+}$ *ssg7*$^{+/-}$	*ssg4*$^{+/-}$ *ssg7*$^{+/-}$		
WT × *ssg4*$^{+/-}$ *ssg7*$^{-/-}$	41	4	30.42 (3.48×10^{-9})	9.76%
ssg4$^{+/-}$ *ssg7*$^{-/-}$ × WT	50	41	0.89 (3.345)	82%

(b)
Genetic analysis of gametic transmission efficiency of heterozygous *ssg4*$^{-/-}$ *ssg7*$^{+/-}$ plants

Combinations (♀ × ♂)	F_1 genotypes		χ^2value (*P*) for 1:1 segregation	TE
	ssg4$^{+/-}$ *ssg7*$^{+/+}$	*ssg4*$^{+/-}$ *ssg7*$^{+/-}$		
WT × *ssg4*$^{-/-}$ *ssg7*$^{+/-}$	34	2	28.44 (9.64×10^{-8})	5.88%
ssg4$^{-/-}$ *ssg7*$^{+/-}$ × WT	52	49	0.089 (0.765)	94.23%

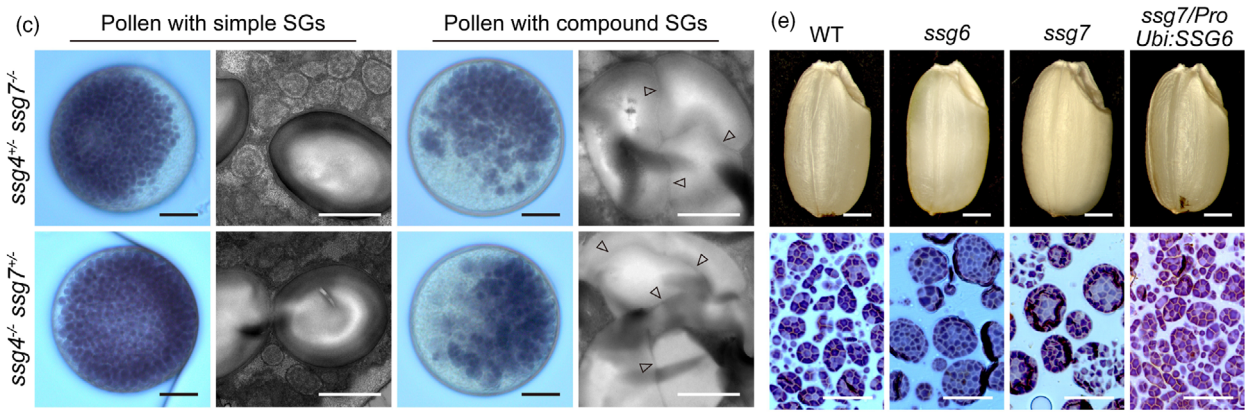

(d)
Segregation of pollen grains with simple and compound SGs

Parental genotype	No. of pollen grains with simple SGs	No. of pollen grains with compound SGs	χ^2 value (*P*) for 1:1 segregation
ssg4$^{+/-}$ *ssg7*$^{-/-}$	154	140	0.668 (0.414)
ssg4$^{-/-}$ *ssg7*$^{+/-}$	89	106	1.493 (0.222)

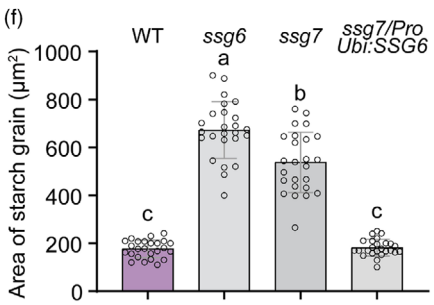

Figure 7 *SSG7* genetically interacts with *SSG4* and *SSG6*. (a) Genetic analysis of gametic transmission efficiency of heterozygous *ssg4*$^{+/-}$ *ssg7*$^{-/-}$ plants. TE, transmission efficiency; WT, wild type. (b) Genetic analysis of gametic transmission efficiency of heterozygous *ssg4*$^{-/-}$ *ssg7*$^{+/-}$ plants. (c) Iodine-stained images and transmission electron microscopy (TEM) images of pollen from heterozygous *ssg4*$^{+/-}$ *ssg7*$^{-/-}$ and *ssg4*$^{-/-}$ *ssg7*$^{+/-}$ plants. Arrowheads indicate gaps between starch granules. Bars = 10 μm in iodine-stained images, 1 μm in TEM images. SG, starch grain. (d) Segregation of pollen with simple and compound SGs from heterozygous *ssg4*$^{+/-}$ *ssg7*$^{-/-}$ and *ssg4*$^{-/-}$ *ssg7*$^{+/-}$ plants. (e, f) Appearance (e) and SG sizes (f) of WT, *ssg6*, *ssg7*, and *SSG6* overexpressed grains (in the *ssg7* background). $P < 0.05$ by Duncan's multiple range tests ($n = 25$). Note that the quantification does not contain the very small SGs.

the chain-length distribution of amylopectin in *ssg7* endosperm starch was markedly altered compared to the almost normal fine structure of amylopectin in *ssg4* and *ssg6* (Figure S1d; Matsushima *et al.*, 2014, 2016). On the other hand, we could not obtain homozygous null mutants of *SSG7* (Figure S7), suggesting that the *ssg7* mutation in this study corresponds to a leaky mutation (Figure 3). Notably, half of the pollen grains from the heterozygous *KO2* line of *SSG7* contained enlarged compound SGs, although normal pollen contained simple SGs (Figure S7c,d). Altogether, these findings indicate that *SSG7* has unique effects on starch biosynthesis and compound SG formation in rice.

SSG7 encodes an amyloplast membrane-localized protein homologous to AtCRL

SSG7 encodes a DUF1001 domain-containing protein homologous to AtCRL (Figures 3 and S9; Asano *et al.*, 2004). The *AtCRL* gene was originally identified by an Arabidopsis mutant showing morphological abnormalities in many vegetative organs and developing enlarged plastids (Asano *et al.*, 2004). Although AtCRL is homologous to the cyanobacterial CpcT lyases (Shen *et al.*, 2006), it seems that the PCB-binding ability of AtCRL is not functionally associated with the *crl* mutant phenotypes (Wang *et al.*, 2020). Therefore, the precise molecular function of *AtCRL* remains elusive, despite the striking *crl*-induced lesions (Li *et al.*, 2020). The genome of the moss *Physcomitrium patens* harbours two homologues of *AtCRL*, *PpCRL1*, and *PpCRL2*, which play redundant roles in plastid division and plant growth. However, PpCRLs do not affect the orientation of the cell division plane, and AtCRL only partially rescued the defects in the plastid division of the *PpCRL* double knockout mutant, highlighting the divergence of CRL function in *P. patens* and Arabidopsis (Sugita *et al.*, 2012).

The DUF1001 domain of SSG7 also possesses four strictly conserved amino acid residues (Figure S9c) that are required for

PCB binding in AtCRL homologues (Wang *et al*., 2020). Consistent with the low sequence identity between SSG7 and CpcT lyase (Figure S9b,c), overexpressing *CpcT* failed to rescue the *ssg7* phenotype (Figure 3e,f). In addition, CpcT does not function as a transporter (Shen *et al*., 2006), whereas AtCRL homologues in plants might have evolved other functions, including protein import (Fang *et al*., 2022). Moreover, *SSG7* is functionally divergent from *AtCRL*, as evidenced by the abnormal SGs in *AtCRL*-overexpressed transgenic plants (Figure 3e,f). As rice mutants defective in plastid division do not develop enlarged SGs (Yun and Kawagoe, 2009, 2010), *SSG7* may not directly function in plastid division, in contrast to *AtCRL* and *PpCRLs*. Therefore, the functions of plant *CRL* genes have greatly diverged during evolution.

AtCRL localizes to the outer envelope membrane of chloroplasts (Asano *et al*., 2004). Similarly, SSG7 largely co-localized with the amyloplast outer envelope membrane marker OEP7-DsRed but not the inner envelope membrane marker BT1-DsRed (Figure 4a–c). Intriguingly, only GFP-SSG7 (but not SSG7-GFP) rescued the *ssg7* phenotype, whereas only AtCRL-GFP or PpCRL-GFP rescued the phenotypes of their respective mutants. In addition, SSG7 lacks a putative chloroplast transit peptide in its N- and C-termini (Emanuelsson *et al*., 1999; Figure S9a), a characteristic of most plastidial outer envelope membrane proteins (Lee *et al*., 2001).

SSG7, SSG4, and SSG6 form a multivalent molecular module that regulates SG size by associating with translocons

Arabidopsis TIC236, a rice SSG4 homologue, serves as a link between the TOC and TIC complexes by interacting with TOC75 in the chloroplast intermembrane space (Chen *et al*., 2018). The knockdown mutant *tic236-2* develops unevenly sized chloroplasts in mesophyll cells (Fang *et al*., 2022). Nevertheless, the *defective kernel5* (*dek5*) mutant of the maize *SSG4* gene develops enlarged amyloplasts (SGs) and chloroplasts. The *dek5* mutation decreases the amounts of TOC75 and chloroplast envelope transporters, suggesting that *DEK5* functions in plastid membrane biogenesis, thereby facilitating envelope protein accumulation and metabolite transport (Zhang *et al*., 2019).

In our study, we verified a direct interaction between SSG4 and SSG7 *in vivo* and *in vitro* (Figure 5). SSG7 is also associated with TOC components, together with weak binding to TIC110 (Figure 6a,b; Data S1); this is similar to AtCRL, which associates with TIC236 and other translocon components (Fang *et al*., 2022). In addition, the *ssg7* mutation markedly reduced the abundance of TOC components (Figure 6c,d). Notably, SSG4, DEK5, and TIC236 have been proposed to play a conserved role in targeting β-barrel membrane proteins (e.g. TOC75) to the outer envelope of plastids (Zhang *et al*., 2019). SSG7 is also possibly involved in this process due to its direct interaction with SSG4 and TOC components (Figures 5 and 6). This may explain the reduced levels of TOC components in *ssg7* (Figure 6c,d), which likely leads to defective proteins or metabolite transport, as observed in *dek5* (Zhang *et al*., 2019). Supporting this notion, gain-of-function mutations of *TIC236*/*SSG4* increase TIC236 stability and enhance the import of proteins involved in plastid division, leading to the abolishment of *crl*-induced lesions (Fang *et al*., 2022). As we failed to clone the full-length coding sequence of *SSG4*, it is challenging for us to determine whether *SSG4* and *SSG7* have similar genetic effects in rice. However, *ssg4* and *ssg7* indeed acted synergistically to modulate SG development in rice (Figure 7a–c), as previously observed for *ssg4* and *ssg6* (Matsushima *et al*., 2016).

SSG6 localizes to the outer envelope membrane of the amyloplast (Matsushima *et al*., 2016; Matsushima and Hisano, 2019). SSG6 likely interacts with SSG7 transiently, given that only a small amount of SSG6 peptides were detected in the GFP-SSG7 immunoprecipitate (Figure 5b). Our data suggest that SSG4, SSG6, and SSG7 form a multi-protein module required for SG and endosperm development. As *SSG6* overexpression restored the defective SG size and endosperm development of *ssg7* (Figure 7e,f), *SSG6*, and *SSG7* may be functional redundancy in modulating SG size and endosperm development. SSG6 shares high homology with Arabidopsis aminocyclopropane-1-carboxylate synthase10 (ACS10) and ACS12, which are aminotransferases rather than ACS (Matsushima *et al*., 2016; Yamagami *et al*., 2003). It is unlikely that SSG7 regulates SG size by disturbing amino acid metabolism, as the loss of function of the cytosolic alanine aminotransferase OsAlaAT1 did not lead to the production of enlarged SGs in rice endosperm (Yang *et al*., 2015). The biological significance of *SSG6* in this translocon-associated complex is largely unknown. Further work is required to explore the molecular mechanism by which the SSG complex orchestrates SG development, amino acid metabolism, and protein import in the future.

Materials and methods

Plant materials and growth conditions

The *ssg7* mutant was isolated from an *N*-methyl-*N*-nitrosourea-mutagenized pool of *japonica* rice (*Oryza sativa*) cultivar W017. Reciprocal crosses between *ssg7* and W017 were used for genetic analysis. An F_2 population derived from a cross between the *ssg7* (*japonica*) with an *indica* cultivar N22 was used for gene mapping. The *ssg4* mutant with a missense mutation derived from *japonica* rice cultivar W017 was crossed with *ssg7* to generate the *ssg4 ssg7* double mutant. The *ssg6* mutant was generated using CRISPR/Cas9 technology in the W017 background. The wild type, mutants, and transgenic lines were grown in experimental fields during the normal growing seasons at the Chinese Academy of Agricultural Science, Beijing.

Physicochemical properties of the endosperm starch

Husked rice grains were processed with a polisher and ground to fine flour in a miller or directly ground into flour without polishing. The total starch content of mature grains was determined using starch assay kits (Megazyme, Wicklow, Ireland, http://www. megazyme.com). The amylose, protein, and lipid contents were measured as previously described (Kang *et al*., 2005). The chain-length distribution (CLD) pattern of amylopectin was determined following the method previously described (Peng *et al*., 2014). The pasting properties of endosperm starch were measured with a Rapid Visco Analyser (TecMaster RVA, Perten).

Microscopy observation

Scanning electron microscopy of mature grains was performed as described previously (Yan *et al*., 2024). Brown rice was hand-sectioned transversely at the mid-section using a razor blade and coated with gold, followed by observation with a SEM5000 (CIQTEK Co., Ltd, Hefei, China).

Semi-thin sections were prepared from developing grains as previously described (Yan *et al*., 2024). Briefly, developing grains

were transversely cut with a razor blade, and approximately 1 mm^3 blocks were taken and fixed in 0.1 M phosphate buffer (pH 7.4) containing 2.5% (v/v) glutaraldehyde at 4 °C in the dark for 12 h. Samples were dehydrated by an ethanol series [30, 50, 70, 90, and 100% (v/v)] and then embedded in LR White resin (London Resin, 14 388-UC). After polymerization at 65 °C for 3 days, semithin sections (1 μm in thickness) were prepared using an ultramicrotome (Leica microsystems, RM2265), and cytohistological analysis was performed as described previously (Wu *et al*., 2016; Yan *et al*., 2024). Images were taken using a Nikon ECLIPSE80i microscope and the representative images were shown. The areas occupied by SGs and the diameter of starch granules were determined with Image J software (https://imagej.nih.gov/ij/).

For visualization of the subcellular localization of SSG7 in subaleurone cells of developing grains, thick sections were prepared following the method described by Ren *et al*. (2020), with minor modifications. Briefly, freshly dehulled developing rice grains were fixed in 5% (w/v) agarose and cut into slices (60 to 100 μm in thickness) using a Vibrating blade microtome (Leica microsystems; VT-1200S). The fresh slices were immersed into ice-cold phosphate buffer before observation of the fluorescence signals with a laser scanning confocal microscope (Zeiss LSM980).

Immuno-gold electronic microscopy of developing rice grain was performed according to a previously described method (Ren *et al*., 2014). Developing rice grains were dehulled, followed by fixation by high-pressure frozen/freeze substituted. After dehydration, samples were embedded in LOWICRYL HM20 resin via UV light irradiation (AFS2, Leica). Ultrathin sections (~70 nm) were prepared with a Leica EM UC7 microtome. Immunogold labelling was performed using the primary monoclonal anti-GFP antibody in combination with 10-nm gold-coupled secondary antibodies. Images were taken with a transmission electron microscope (Hitachi H7700, Tokyo, Japan).

Map-based cloning of the *SSG7* gene

To map the *SSG7* locus, we constructed an F_2 population by crossing *ssg7* (*japonica*) with *indica* cultivar N22. Individuals with floury endosperm in the F_2 population were used for mapping. Molecular markers were developed based on comparisons of the sequence polymorphism between *japonica* cultivar Nipponbare and *indica* cultivar 93-11 (Table S4).

Plasmid construction and transformation

For complementation test, full-length coding sequence of *SSG7* was amplified and inserted into the *Kpn*I and *BamH*I sites of pCUBi1390 vector to generate the *ProUbi:SSG7* construct. Similarly, the entire coding regions of *SSG6*, Arabidopsis *CRL*, and cyanobacteria *CpcT* were used to generate the *ProUbi:SSG6*, *ProUbi:CRL*, and *ProUbi:CpcT* constructs, respectively. The coding sequence of *Synechococcus elongatus* PCC 6301 *CpcT* (Sugita *et al*., 2007) was synthesized in GeneScript Biotech (Nanjing, China; https://www.genscript.com.cn/).

For the fusion complementation test, the full-length coding sequence of *SSG7* was fused to the N or C terminus of GFP in the binary vector pCAMBIA1305 driven by its native 2114-bp promoter to produce *ProSSG7:SSG7-GFP* and *ProSSG7:GFP-SSG7* constructs, respectively.

To investigate the subcellular localization of SSG7 in the developing endosperm, the full-length coding sequence of *SSG7* was inserted into the *Bgl*II site of the modified binary vector pCAMBIA1305 (hygromycin-resistant; Ren *et al*., 2020) containing a GFP tag driven by the maize *UBIQUITIN* promoter to generate the *ProUbi:GFP-SSG7* construct. For colocalization analyses, the coding sequences of *OEP7* and *BT1* were separately cloned into the *BamH*I site of the modified binary vector pCAMBIA2300 (kanamycin-resistant; Ren *et al*., 2020) containing a DsRed tag driven by the maize *UBIQUITIN* promoter, to generate *ProUbi:OEP7-DsRed* and *ProUbi:BT1-DsRed* constructs. These constructs were separately introduced into transgenic plants harbouring *ProUbi:GFP-SSG7* for colocalization analyses.

To generate a knockout construct, 20-bp gene-specific spacer sequences of the target genes were separately inserted into the CRISPR-Cas9 expression vector following the method described previously (Miao *et al*., 2013).

Unless indicated otherwise, all constructs were separately introduced into W017 or *ssg7* calli via *Agrobacterium*-mediated transformation (Hiei *et al*., 1994). Primers are listed in Table S4.

Protein extraction and immunoblot analyses

Total protein extraction from rice seeds and immunoblot analysis were performed as described previously (Yan *et al*., 2024).

Subcellular fractionation

Subcellular fractionation assay was performed using the methods described previously with minor modifications (Ren *et al*., 2020; Wang *et al*., 2016). Briefly, the wild-type developing grains (9 DAF) were dehulled and homogenized in 2-fold volume (on a basis of fresh weight) of ice-cold extraction buffer A (100 mM HEPS-KOH [pH 7.5], 2 mM $MgCl_2$, 5 mM EGTA, 300 mM sucrose, 1 mM PMSF, 1% [v/v] Triton X-100, and proteinase inhibitor cocktail [Roche]). The homogenate was centrifuged at 200 ***g*** for 10 min at 4 °C to remove starch-rich pellets, followed by filtration through four layers of cheesecloth, and subsequent ultracentrifugation at 100 000 ***g*** for 1 h at 4 °C to obtain the membrane-associated pellet (P100) and soluble supernatant (S100) for immunoblot analyses using the protein-specific antibodies.

The P100 fraction was resuspended in different solutions of buffer A (with the same volume used for initial homogenization), separately containing (1 M NaCl, 0.1 M Na_2CO_3 [pH 11.5], 1% [v/v] Triton X-100, or 1% [v/v] Nonidet P-40). After incubation for 1 h in ice, the resuspending solutions were ultracentrifugated at 100 000 ***g*** for 1 h at 4 °C to obtain the soluble supernatant (S) and insoluble pellet (P), followed by immunoblot analyses.

Immunoprecipitation and mass spectrometry (IP-MS)

Approximately 5 g of developing grains expressing GFP-SSG7 or free GFP were homogenized in a 1.2-fold volume (on a basis of fresh weight) of ice-cold extraction buffer (50 mM Tris-MES [pH 7.5], 1 mM $MgCl_2$, 0.5 M sucrose, 10 mM EDTA, 5 mM DTT, 0.1% [w/v] Nonidet P-40, and proteinase inhibitor cocktail [Roche]). Starch-rich pellets were removed by centrifugation at 200 ***g*** for 10 min at 4 °C, and the resultant supernatant was filtered through four layers of cheesecloth, followed by incubation with μMACS Microbeads conjugated to anti-GFP (Miltenyi Biotec; 30-091-125) for 1 h at 4 °C. After incubation, the mixture was filtered using a μColumn that is adsorbed on a magnetic stand (Miltenyi Biotec). The μColumn was washed three times with the extraction buffer containing 0.2% (v/v) Nonidet P-40. The bound proteins were eluted with 80 μL elution buffer (50 mM Tris–HCl [pH 6.8], 50 mM DTT, 1% [w/v] SDS, 1 mM EDTA, 0.005% [w/v] bromphenol blue and 10% [v/v] glycerol). Mass spectrometry analyses and data collection were conducted as

previously described by Ren *et al*. (2020). Three independent experiments were performed.

In vivo co-immunoprecipitation (Co-IP) assay

In vivo co-immunoprecipitation assay in rice protoplasts was performed as previously described by Chen *et al*. (2006) with minor modifications. Rice protoplasts were prepared from the leave sheath of 10-day-old seedlings. The full-length coding sequence of *SSG7* was separately cloned into pAN580 (containing a GFP tag) and pCAMBIA1300-221-Flag vectors (containing a Flag tag) to generate GFP-SSG7 and Flag-SSG7 fusion constructs. Various combinations of plasmids were transiently co-expressed in rice protoplasts. On the second day after incubation, total protein was extracted from co-expressed rice protoplasts using ice-cold protein lysis buffer (50 mM Hepes [pH 7.5], 150 mM KCl, 10 mM EDTA, 1 mM DTT, 0.4% [v/v] Triton X-100, and proteinase inhibitor cocktail [Roche]), followed by centrifugation and incubation with 20 μL of anti-GFP mAb-Magnetic beads (MBL, D153-10) for 1 h at 4 °C with shaking. Before elution of the bound proteins with a reducing buffer (50 mM Tris–HCl [pH 6.8], 100 mM DTT, 2% [w/v] SDS, 3% [v/v] glycerol, and 0.005% [w/v] bromophenol blue), the beads were washed three times with extraction buffer. The immunoprecipitate samples were subjected to SDS-PAGE and immunoblotting analyses using anti-GFP (dilution 1 : 5000) and anti-Flag antibodies (dilution 1 : 5000), respectively.

In vitro pull-down assay

Partial coding sequence of *SSG7* (encoding amino acids 56 to 275) was inserted into the pGEX-4T-2 vector at the *BamH*I and *EcoR*I sites to generate GST-DUF1001 construct. Partial coding sequence of *SSG4* (encoding amino acids 1730 to 2119 or 2135) was inserted into the pET-30a vector at the *BamH*I and *EcoR*I sites to generate the His-DUF490Δ and His-DUF490 constructs, respectively. These constructs were transformed into *Escherichia coli* strain Rosetta (DE3) and after induction, recombinant proteins were purified using the His beads (Beaver; 70501-100) or GST beads (Beaver; 70601-100), following the manufacturer's instructions. Equal amounts (~2 μg) of GST and GST-DUF1001 protein were separately incubated with 20 μL of GST beads in 1-mL binding buffer (50 mM Tris–HCl [pH 7.5], 100 mM NaCl, 0.5% [v/v] Triton X-100, and proteinase inhibitor cocktail [Roche]) at 4 °C for 1 h. The supernatant was collected and separately mixed with approximately 2 μg of purified His-DUF490 or His-DUF490Δ fusion proteins, and then incubated at 4 °C for another 2 h. After washing beads at least 5 times with the binding buffer, the bound proteins were eluted with equal volumes of SDS sample buffer and subjected to SDS-PAGE immunodetection using anti-GST (dilution 1 : 5000) and anti-His (dilution 1 : 5000) antibodies. Three independent experiments were performed and similar results were obtained. The relative amounts of His fusion proteins bound to GST-DUF1001 were calculated using Image J software (https://imagej.nih.gov/ij/).

Firefly luciferase complementation imaging (LCI) assay

Full-length coding sequence of *SSG6*, *SSG7* and *BT1* was N terminally fused to nLUC in the pCAMBIA-nLUC vector to generate the SSG6-nLUC, SSG7-nLUC, and BT1-nLUC constructs, respectively. Full-length coding sequence of *SSG7* and BT1 was fused to cLUC in the pCAMBI-cLUC vector to generate the SSG7-cLUC and BT1-cLUC constructs, respectively. Different combinations of EHA105 strains containing transformed plasmids were co-infiltrated into leaves of *N. benthaminana*. After 2 days, the relative LUC activity was calculated by a Plant Molecular Imaging System *in vivo* as described previously by Chen *et al*. (2008). Three independent experiments were performed and representative images were shown.

Yeast two-hybrid assay

The sequence encoding the SSG7 variant with a deletion of the TM domain was cloned into the pGADT7 and pGBKT7 vectors at *Xba*I and *BamH*I sites to generate AD-SSG7(ΔTM) and BD-SSG7 (ΔTM) constructs, respectively. Various combinations of plasmids were cotransformed into yeast strain AH109, followed by the screening of interactions according to the manufacturer's instructions. The experiments were repeated twice independently and similar results were obtained.

Antibodies

Partial coding sequence of *SSG7* (amino acids 50 to 242), *SSG6* (amino acids 1 to 195), *TOC159* (amino acids 1 to 150), and *TOC34* (amino acids 1 to 312) were separately cloned into expression vector pET-28a at *BamH*I and *EcoR*I sites for recombinant proteins expression. Recombinant proteins were extracted and purified using the crude extracts from transformed *E. coli* strain Rosetta (DE3), with the His beads (Beaver; 70501-100). Synthetic peptides of TOC75 (C-FERVDLEGKAK) were synthesized. The purified recombination proteins (approximately 1 mg) or synthetic peptides were injected into rabbits for polyclonal antibody production at ABclonal biotechnology (Wuhan, China; https://abclonal.com.cn/). Anti-TIC110 antibodies were prepared as described previously (Zhu *et al*., 2018). Anti-EF-1α (Agrisera, AS10 934), anti-GST (MBL, PM013-7), anti-His (MBL, D291-7), anti-GFP (Roche, 11 814 460 001), and anti-Flag (Sigma, A8592) antibodies are commercially available and diluted at 1 : 5000.

Accession numbers

Sequence data from this article can be found in the GenBank/EMBL databases under the following accession numbers: SSG7 (LOC_Os11g32160), SSG4 (LOC_Os01g08420), SSG6 (LOC_Os06g03990), TOC159 (LOC_Os05g05950), TOC120 (LOC_Os10g40110), TOC90 (LOC_Os12g09570), TOC75 (LOC_Os03g16440), TOC64 (LOC_Os03g50010), TOC34 (LOC_Os03g13730), and TIC110 (LOC_Os10g35010). Accession numbers for the proteins used in phylogenetic tree construction were listed on the tree.

Acknowledgements

This work was supported by National Key R&D Program of China (2021YFF1000200), Innovation Program of Chinese Academy of Agricultural Sciences, Key R&D Program of Jiangsu Province (BE2021359), and Central Public-Interest Scientific Institution Basal Research Fund, China (Y2021YJ18 and S2020YC05). We also gratefully thank Dr. Fan Wang and Jianan Wu from the Core Facility Platform, Chinese Academy of Agriculture Science (CAAS) for their assistance with SEM analysis.

Conflicts of interest

The authors declare no conflict of interest.

Author contributions

J.M.W. and W.W.Z. designed the project. H.G.Y., Y.H.W., B.L.Z., J.J., Z.J., X.Z., and Y.Z. performed the experiments. Other authors provided technical support; W.W.Z., Y.H.W., Y.L.R., and H.G.Y wrote the manuscript.

Data availability statement

Data sharing not applicable to this article as no datasets were generated or analysed during the current study.

References

Asano, T., Yoshioka, Y., Kurei, S., Sakamoto, W., Sodmergen and Machida, Y. (2004) A mutation of the *CRUMPLED LEAF* gene that encodes a protein localized in the outer envelope membrane of plastids affects the pattern of cell division, cell differentiation, and plastid division in Arabidopsis. *Plant J.* **38**, 448–459.

Chen, S.B., Tao, L.Z., Zeng, L.R., Vega-Sanchez, M.E., Umemura, K. and Wang, G.L. (2006) A highly efficient transient protoplast system for analyzing defence gene expression and protein-protein interactions in rice. *Mol. Plant Pathol.* **7**, 417–427.

Chen, H., Zou, Y., Shang, Y., Lin, H., Wang, Y., Cai, R., Tang, X. *et al*. (2008) Firefly luciferase complementation imaging assay for protein-protein interactions in plants. *Plant Physiol.* **146**, 368–376.

Chen, Y.L., Chen, L.J., Chu, C.C., Huang, P.K., Wen, J.R. and Li, H.M. (2018) TIC236 links the outer and inner membrane translocons of the chloroplast. *Nature* **564**, 125–129.

Crumpton-Taylor, M., Grandison, S., Png, K.M., Bushby, A.J. and Smith, A.M. (2012) Control of starch granule numbers in Arabidopsis chloroplasts. *Plant Physiol.* **158**, 905–916.

Emanuelsson, O., Nielsen, H. and Von Heijne, G. (1999) ChloroP, a neural network-based method for predicting chloroplast transit peptides and their cleavage sites. *Protein Sci.* **8**, 978–984.

Fang, J., Li, B., Chen, L.J., Dogra, V., Luo, S., Wu, W., Wang, P. *et al*. (2022) *TIC236* gain-of-function mutations unveil the link between plastid division and plastid protein import. *Proc. Natl. Acad. Sci. USA* **119**, e2123353119.

Gutiérrez, O.A., Campbell, M.R. and Glover, D.V. (2002) Starch particle volume in single- and double-mutant maize endosperm genotypes involving the soft starch (*h*) gene. *Crop Sci.* **42**, 355–359.

Hiei, Y., Ohta, S., Komari, T. and Kumashiro, T. (1994) Efficient transformation of rice (*Oryza sativa* L.) mediated by *Agrobacterium* and sequence analysis of the boundaries of the T-DNA. *Plant J.* **6**, 271–282.

Huang, L., Tan, H., Zhang, C., Li, Q. and Liu, Q. (2021) Starch biosynthesis in cereal endosperms: an updated review over the last decade. *Plant Commun.* **2**, 100237.

Jackson, D.T., Froehlich, J.E. and Keegstra, K. (1998) The hydrophilic domain of Tic110, an inner envelope membrane component of the chloroplastic protein translocation apparatus, faces the stromal compartment. *J. Biol. Chem.* **273**, 16583–16588.

James, M.G., Denyer, K. and Myers, A.M. (2003) Starch synthesis in the cereal endosperm. *Curr. Opin. Plant Biol.* **6**, 215–222.

Jane, J.-L., Kasemsuwan, T., Leas, S., Ames, I.A., Zobel, H., Darien, I.L. *et al*. (1994) Anthology of starch granule morphology by scanning electron microscopy. *Starch-Starke* **46**, 121–129.

Jarvis, P. and López-Juez, E. (2013) Biogenesis and homeostasis of chloroplasts and other plastids. *Nat. Rev. Mol. Cell Biol.* **14**, 787–802.

Jobling, S. (2004) Improving starch for food and industrial applications. *Curr. Opin. Plant Biol.* **7**, 210–218.

Kang, H.G., Park, S., Matsuoka, M. and An, G.H. (2005) White-core endosperm *floury endosperm-4* in rice is generated by knockout mutations in the C_4-type pyruvate orthophosphate dikinase gene (*OsPPDKB*). *Plant J.* **42**, 901–911.

Kawagoe, Y. (2013) The characteristic polyhedral, sharp-edged shape of compound-type starch granules in rice endosperm is achieved via the septum-like structure of the amyloplast. *J. Appl. Glycosci.* **60**, 29–36.

Krogh, A., Larsson, B., von Heijne, G. and Sonnhammer, E.L.L. (2001) Predicting transmembrane protein topology with a hidden Markov model: application to complete genomes. *J. Mol. Biol.* **305**, 567–580.

Lee, Y.J., Kim, D.H., Kim, Y.W. and Hwang, I. (2001) Identification of a signal that distinguishes between the chloroplast outer envelope membrane and the endomembrane system in vivo. *Plant Cell* **13**, 2175–2190.

Li, B.Q., Fang, J., Singh, R.M., Zi, H.L., Lv, S.S., Liu, R.Y., Dogra, V. *et al*. (2020) FATTY ACID DESATURASE5 is required to induce autoimmune responses in gigantic chloroplast mutants of Arabidopsis. *Plant Cell* **32**, 3240–3255.

Lindeboom, N., Chang, P.R. and Tyler, R.T. (2004) Analytical, biochemical and physicochemical aspects of starch granule size, with emphasis on small granule starches: a review. *Starch-Starke* **56**, 89–99.

Malinski, E., Daniel, J.R., Zhang, X.X. and Whistler, R.L. (2003) Isolation of small starch granules and determination of their fat mimic characteristics. *Cereal Chem.* **80**, 1–4.

Matsushima, R. and Hisano, H. (2019) Imaging amyloplasts in the developing endosperm of barley and rice. *Sci. Rep.* **9**, 3745.

Matsushima, R., Maekawa, M., Fujita, N. and Sakamoto, W. (2010) A rapid, direct observation method to isolate mutants with defects in starch grain morphology in rice. *Plant Cell Physiol.* **51**, 728–741.

Matsushima, R., Maekawa, M., Kusano, M., Kondo, H., Fujita, N., Kawagoe, Y. and Sakamoto, W. (2014) Amyloplast-localized SUBSTANDARD STARCH GRAIN4 protein influences the size of starch grains in rice endosperm. *Plant Physiol.* **164**, 623–636.

Matsushima, R., Maekawa, M., Kusano, M., Tomita, K., Kondo, H., Nishimura, H., Crofts, N. *et al*. (2016) Amyloplast membrane protein SUBSTANDARD STARCH GRAIN6 controls starch grain size in rice endosperm. *Plant Physiol.* **170**, 1445–1459.

Miao, J., Guo, D.S., Zhang, J.Z., Huang, Q.P., Qin, G.J., Zhang, X., Wan, J.M. *et al*. (2013) Targeted mutagenesis in rice using CRISPR-Cas system. *Cell Res.* **23**, 1233–1236.

Peng, C., Wang, Y.H., Liu, F., Ren, Y.L., Zhou, K.N., Lv, J., Zheng, M. *et al*. (2014) *FLOURY ENDOSPERM6* encodes a CBM48 domain-containing protein involved in compound granule formation and starch synthesis in rice endosperm. *Plant J.* **77**, 917–930.

Ren, Y.L., Wang, Y.H., Liu, F., Zhou, K.N., Ding, Y., Zhou, F., Wang, Y. *et al*. (2014) *GLUTELIN PRECURSOR ACCUMULATION3* encodes a regulator of post-Golgi vesicular traffic essential for vacuolar protein sorting in rice endosperm. *Plant Cell* **26**, 410–425.

Ren, Y.L., Wang, Y.H., Pan, T., Wang, Y.L., Wang, Y.F., Gan, L., Wei, Z.Y. *et al*. (2020) *GPA5* encodes a Rab5a effector required for post-Golgi trafficking of rice storage proteins. *Plant Cell* **32**, 758–777.

Richardson, L.G.L. and Schnell, D.J. (2020) Origins, function, and regulation of the TOC-TIC general protein import machinery of plastids. *J. Exp. Bot.* **71**, 1226–1238.

Roldan, I., Wattebled, F., Mercedes Lucas, M., Delvalle, D., Planchot, V., Jimenez, S., Perez, R. *et al*. (2007) The phenotype of soluble starch synthase IV defective mutants of *Arabidopsis thaliana* suggests a novel function of elongation enzymes in the control of starch granule formation. *Plant J.* **49**, 492–504.

Selkrig, J., Mosbahi, K., Webb, C.T., Belousoff, M.J., Perry, A.J., Wells, T.J., Morris, F. *et al*. (2012) Discovery of an archetypal protein transport system in bacterial outer membranes. *Nat. Struct. Mol. Biol.* **19**, 506–510.

Seung, D. and Smith, A.M. (2019) Starch granule initiation and morphogenesis-progress in Arabidopsis and cereals. *J. Exp. Bot.* **70**, 771–784.

Seung, D., Boudet, J., Monroe, J., Schreier, T.B., David, L.C., Abt, M., Lu, K.J. *et al*. (2017) Homologs of PROTEIN TARGETING TO STARCH control starch granule initiation in Arabidopsis leaves. *Plant Cell* **29**, 1657–1677.

Seung, D., Schreier, T.B., Burgy, L., Eicke, S. and Zeeman, S.C. (2018) Two plastidial coiled-coil proteins are essential for normal starch granule initiation in Arabidopsis. *Plant Cell* **30**, 1523–1542.

Shen, G., Saunee, N.A., Williams, S.R., Gallo, E.F., Schluchter, W.M. and Bryant, D.A. (2006) Identification and characterization of a new class of bilin lyase - the *cpcT* gene encodes a bilin lyase responsible for attachment of phycocyanobilin to CYS-153 on the β-subunit of phycocyanin in *synechococcus sp* PCC 7002. *J. Biol. Chem.* **281**, 17768–17778.

Sugita, C., Ogata, K., Shikata, M., Jikuya, H., Takano, J., Furumichi, M., Kanehisa, M. *et al*. (2007) Complete nucleotide sequence of the freshwater

unicellular cyanobacterium *Synechococcus elongatus* PCC 6301 chromosome: gene content and organization. *Photosynth. Res.* **93**, 55–67.
Sugita, C., Kato, Y., Yoshioka, Y., Tsurumi, N., Iida, Y., Machida, Y. and Sugita, M. (2012) *CRUMPLED LEAF* (*CRL*) homologs of *Physcomitrella patens* are involved in the complete separation of dividing plastids. *Plant Cell Physiol.* **53**, 1124–1133.
Vandromme, C., Spriet, C., Dauvillée, D., Courseaux, A., Putaux, J.L., Wychowski, A., Krzewinski, F. *et al*. (2019) PII1: a protein involved in starch initiation that determines granule number and size in Arabidopsis chloroplast. *New Phytol.* **221**, 356–370.
Wang, Y.H., Liu, F., Ren, Y.L., Wang, Y.L., Liu, X., Long, W.H., Wang, D. *et al*. (2016) GOLGI TRANSPORT 1B regulates protein export from the endoplasmic reticulum in rice endosperm cells. *Plant Cell* **28**, 2850–2865.
Wang, F., Fang, J., Guan, K., Luo, S., Dogra, V., Li, B., Ma, D. *et al*. (2020) The Arabidopsis CRUMPLED LEAF protein, a homolog of the cyanobacterial bilin lyase, retains the bilin-binding pocket for a yet unknown function. *Plant J.* **104**, 964–978.
Wang, R.Q., Ren, Y.L., Yan, H.G., Teng, X., Zhu, X.P., Wang, Y.P., Zhang, X. *et al*. (2021) ENLARGED STARCH GRAIN1 affects amyloplast development and starch biosynthesis in rice endosperm. *Plant Sci.* **305**, 110831.
Wilson, J.A., Glover, D.V. and Nyquist, W.E. (2000) Effect of dosage at the soft starch (*h*) locus on starch granule volume in maize. *Plant Breed.* **119**, 177–178.
Wu, X.B., Liu, J.X., Li, D.Q. and Liu, C.M. (2016) Rice caryopsis development I: dynamic changes in different cell layers. *J. Integr. Plant Biol.* **58**, 772–785.
Yamagami, T., Tsuchisaka, A., Yamada, K., Haddon, W.F., Harden, L.A. and Theologis, A. (2003) Biochemical diversity among the 1-amino-cyclopropane-1-carboxylate synthase isozymes encoded by the *Arabidopsis* gene family. *J. Biol. Chem.* **278**, 49102–49112.
Yan, H., Zhang, W., Wang, Y., Jin, J., Xu, H., Fu, Y., Shan, Z. *et al*. (2024) Rice LIKE EARLY STARVATION1 cooperates with FLOURY ENDOSPERM6 to modulate starch biosynthesis and endosperm development. *Plant Cell* **36**, 1892–1912.
Yang, J., Kim, S.R., Lee, S.K., Choi, H., Jeon, J.S. and An, G. (2015) Alanine aminotransferase 1 (OsAlaAT1) plays an essential role in the regulation of starch storage in rice endosperm. *Plant Sci.* **240**, 79–89.
Yun, M.S. and Kawagoe, Y. (2009) Amyloplast division progresses simultaneously at multiple sites in the endosperm of rice. *Plant Cell Physiol.* **50**, 1617–1626.
Yun, M.S. and Kawagoe, Y. (2010) Septum formation in amyloplasts produces compound granules in the rice endosperm and is regulated by plastid division proteins. *Plant Cell Physiol.* **51**, 1469–1479.
Zhang, J., Wu, S., Boehlein, S.K., McCarty, D.R., Song, G., Walley, J.W., Myers, A. *et al*. (2019) Maize *defective kernel5* is a bacterial TamB homologue required for chloroplast envelope biogenesis. *J. Cell Biol.* **218**, 2638–2658.
Zhao, L.X., Pan, T., Guo, D.W. and Wei, C.X. (2018) A simple and rapid method for preparing the whole section of starchy seed to investigate the morphology and distribution of starch in different regions of seed. *Plant Methods* **14**, 16.
Zhu, X., Teng, X., Wang, Y., Hao, Y., Jing, R., Wang, Y., Liu, Y. *et al*. (2018) *FLOURY ENDOSPERM11* encoding a plastid heat shock protein 70 is essential for amyloplast development in rice. *Plant Sci.* **277**, 89–99.

Supporting information

Additional supporting information may be found online in the Supporting Information section at the end of the article.

Data S1 Summary of proteins co-precipitated with GFP-SSG7 and identified by mass spectrometry.
Figure S1 *ssg7* impaired endosperm development.
Figure S2 Quantification of the numbers of starch grains and starch granules.
Figure S3 The appearance of endosperm and the sizes of starch grains (SGs) of F_1 grains from reciprocal crosses.
Figure S4 Starch grains (SGs) in pollen grains and pericarp cells.
Figure S5 Chloroplast morphologies in *ssg7* leaves.
Figure S6 Overexpression of *SSG7* driven by the *UBIQUITIN* promoter specifically rescued the *ssg7* mutant phenotypes.
Figure S7 Characterization of *SSG7* knockout mutants.
Figure S8 The expression level of *SSG7* in *ssg7* developing endosperm.
Figure S9 Structure and phylogenetic analyses and amino acid sequence alignment of the SSG7 protein.
Figure S10 Complementation of *ssg7* by expressing GFP-tagged SSG7 fusion protein.
Figure S11 Rescue of *ssg7* mutant phenotype by overexpressing the GFP-SSG7 fusion protein.
Figure S12 Phenotypes of the *ssg4* mutant.
Figure S13 Rescue of *ssg7* defective phenotype by overexpressing *SSG6*.
Figure S14 Assessment of the specificity of polyclonal antibodies generated in this work.
Table S1 Agronomic traits of the wild type (WT), *ssg* mutants, and transgenic plants.
Table S2 Genetic analysis of the *ssg7* mutant.
Table S3 Segregation analysis of progenies from double heterozygous $ssg4^{+/-}$ $ssg7^{+/-}$ plants.
Table S4 Primers used in this study.